Reconstruction of transverse-longitudinal vibrations in the organ of Corti complex via optical coherence tomography

Brian L. Frost,[1] Clark Elliott Strimbu,[2] and Elizabeth S. Olson[3]

[1]*Department of Electrical Engineering, Columbia University, 500 W. 120th St.,*

Mudd 1310, New York, NY 1002, USA.[a]

[2]*Department of Otolaryngolgy Head and Neck Surgery,*

Vagelos College of Physicians and Surgeons, Columbia University, 630 W 168th St,

New York, NY 10032.

[3]*Department Biomedical Engineering, Columbia University,*

351 Engineering Terrace, 1210 Amsterdam Avenue,New York,

NY 10027. Also at Department of Otolaryngolgy Head and Neck Surgery.

(Dated: 13 August 2022)

---

[a]b.frost@columbia.edu

I. INTRODUCTION

Optical coherence tomography (OCT) is a powerful instrument for the study of cochlear mechanics. It is capable both of volumetric imaging and sub-nanometer vibrometry at a depth into a sample[1,2], allowing for the measurement of motion inside of the organ of Corti complex (OCC) *in vivo*[3–9]. These data have provide significant insight into OCC micromechanics, both improving our understanding of and raising many questions about the mechanisms responsible for the incredible dynamic range of the sensitive cochlea. However, certain limitations of OCT can greatly complicate the interpretation of these data.
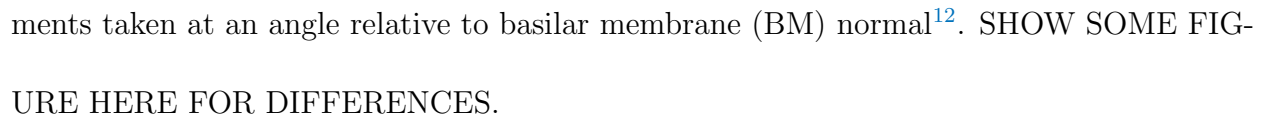
OCT vibration measurements and images are built from one-dimensional axial scans (A-Scans), generated via the Fourier transform of raw photodetector data. The magnitude of the A-Scan indicates the reflectivity at different depths into the sample. Images (referred to as brightness scans, or B-Scans) are built by taking a series of A-Scans along a line perpendicular to the optical axis. Many parallel B-Scans can be taken to form a volume scan.

A series of A-Scans at one location is referred to as a motion scan (M-Scan). The phase of a single pixel as a function of time is proportional to the sub-pixel displacement *along the axis of the beam* of structures at that position[2]. That is, an M-Scan allows us to measure a projection of the 3-D motion of a structure onto the beam axis.

The nature of the modality leads to several important complications: (1) as OCT images are based on reflectivity, they are *label-free*, so structures must be identified via known anatomy and intuition; (2) displacement measurements are 1-D projections of 3-D motions.

These issues are even further complicated by the fact that the optical axis is often decided via the constraints of the preparation, and its relationship to the anatomy is often not known *a priori.*

We have discussed these issues in terms of the anatomical coordinates of the cochlea (longitudinal, radial and transverse), using volume scans to determine the optical axis' relation to more physiologically relevant axes[10]. Using this method, one can account for the longitudinal (tonotopic) distance between measured points in a single A-Scan. One can also determine which components of motion are most represented in a measurement, offering more context to reported results. However, even this is not sufficient to separate out the motion components themselves.

It has been shown by Cooper et al that viewing angle can significantly impact both the magnitude and phase response of the structures being measured[11]. For example, purely transverse measurements in the gerbil base have shown different character than measurements taken at an angle relative to basilar membrane (BM) normal[12]. SHOW SOME FIGURE HERE FOR DIFFERENCES.

Recent efforts have been made to better understand intra-OCC motion at anatomically relevant angles, as these measurements could better aid in our understanding of cochlear micromechanics. For example, radial motion of the tectorial mebrane and stereocilia is responsible for the transduction that results in neural responses and electromotility in inner and outer hair cells, respectively. Longitudinal motion may clarify the impact of fluid motion intra-OCC, where cells may not simply move as rigid bodies.

One possible solution is to measure motion directly at an angle of interest. For example, Cho et al have measured at a transverse angle in the hook region of the gerbil base, and Ren et al have similarly made purely transverse measurements of the reticular lamina in the gerbil base. Preliminary work has also been done to make exclusively radial measurements of intra-OCC motion in mouse. However, such measurement angles are not available in certain preparations, dependent on species and frequency location of interest.

Other methods have been developed to reconstruct motion along physiologically relevant axes without directly measuring along any of these axes explicitly. Lee et al used back-projection of measurements taken at two different angles to reconstruct radial-transverse motion in mouse, via carefully rotating the preparation to ensure they stay in the same cross-section[8]. Kim et al used a three-beam OCT system in mouse to measure motion at the same location from three angles, and back-project to resolve three-dimensional motion CITE. These methods are challenging to implement in the gerbil base, where the anatomy and opacity of the bone significantly restricts the beam angle when viewing through the round window (RW). The latter method also requires significant hardware and space.

We have developed a method to reconstruct the longitudinal and transverse components of motion *in vivo* via OCT. Similar to the work described above, we reconstruct via back-projecting measurements taken at two angles. However, our method performs registration via *physiology* rather than mechanical precision – our method requires no *a priori* knowledge of either measurement angle, or of the precise positions of the structures being measured. Instead we use the traveling wave phase on the BM, along with a simplified version of the orientation program presented in Frost et al, 2022, to register intra-OCC positions between

65 viewing angles. This allows the method to work in any species or preparation, including in

66 the gerbil base in which we are particularly interested.

67 We present the method, an analysis of the accuracy of this method as a function of

68 angular distance between viewing angles, and *in vivo* experimental data taken through the

69 RW in gerbil. We present longitudinal and transverse motion at the outer hair cell/Deiters'

70 cell junction (OHC-DC), and see that the transverse data matches well with previously

71 measured purely transverse motion in the gerbil base. In particular, we see that transverse

72 OHC-DC motion phase lags BM motion phase across frequency by 0.3 cycles, save at high

73 SPL where the two seem to move in-phase. This is in stark contrast with motion measured

74 at an angle with a longitudinal component, where a broadband phase lead of OHC-DC re

75 BM is often seen[10].

II. METHODS

77 In this section, we will present our method for reconstructing transverse-longitudinal

78 motion in the OCC. To begin, we will present the mathematical basis for this method.

79 Then, we will describe the experimental process by which the quantities required for the

80 reconstruction are acquired.

A. Mathematics of reconstruction

82 The true motion of each structure is three-dimensional. However, in this work, we are

83 only concerned with longitudinal and transverse motion components. Ensuring that our

84 measurement angles have no radial component, we can consider the "true motion" of a single

85 point of interest as being a two-dimensional vector. Call the longitudinal and transverse unit

86 vectors $\hat{\mathbf{l}}$ and $\hat{\mathbf{t}}$, respectively. The true displacement can be written as a two-vector with

87 longitudinal and transverse components as

$$\mathbf{d} = d_l\hat{\mathbf{l}} + d_t\hat{\mathbf{t}}. \tag{1}$$

88

89 Our beam axis is a unit vector that can also be written in anatomical coordinates, having

90 a transverse and longitudinal component. Consider two such beam axes,

$$\mathbf{z}_1 = l_1\hat{\mathbf{l}} + t_1\hat{\mathbf{t}}, \ \ \mathbf{z}_2 = l_2\hat{\mathbf{l}} + t_2\hat{\mathbf{t}}. \tag{2}$$

91

92 We take measurements of the point of interest along both of these axes, δ_1 and δ_2. These

93 are 1-D displacements, defined as the projection of the true motion $\mathbf{d}$ onto $\mathbf{z}_1$ and $\mathbf{z}_2$,

94 respectively. Mathematically, this relationship is described as a dot product:

$$\delta_i = \mathbf{z}_i^T\mathbf{d}, \ i = 1, 2. \tag{3}$$

95 We can also write this as a system of two equations in matrix form as

$$\begin{pmatrix} \delta_1 \\ \delta_2 \end{pmatrix} = \begin{pmatrix} l_1 & t_1 \\ l_2 & t_2 \end{pmatrix} \begin{pmatrix} d_l \\ d_t \end{pmatrix}, \tag{4}$$

96 or to solve for $\mathbf{d}$,

$$\begin{pmatrix} d_l \\ d_t \end{pmatrix} = \begin{pmatrix} l_1 & t_1 \\ l_2 & t_2 \end{pmatrix}^{-1} \begin{pmatrix} \delta_1 \\ \delta_2 \end{pmatrix}. \tag{5}$$

97

98 Our goal is to reconstruct the 2-D motion, i.e. to find $\mathbf{d}$. To solve for $\mathbf{d}$, we need

99 to measure δ_1 and δ_2 *at the same location*, and we need to find anatomical coordinate

100 representations of the measurement axes (i.e. the elements of the 2×2 matrix in Eq. 5).

B.   Experimental method

To perform the reconstruction according to Eq. 5, we must be able to (1) determine the measurement axes in anatomical coordinates (l_i and t_i), and (2) register a point of interest between two orientations so that the *same structure* may be measured at both angles. We present a method that performs both of these tasks without any *a priori* knowledge of precise location structures or beam angles, using only a single OCT system and the traveling wave physiology of the mammallian cochlea. Each step is also presented visually in a panel in FIGURE.

We begin with our OCT system viewing the OCC at some unknown angle with respect to the BM normal. Using the ThorLabs ThorImage software, we are able to view a real-time volume scan of the sample at this angle. Doing so, we note two points in the volume which lie on the same anatomical structure, and refer to their 3-D coordinates as $\mathbf{p}_1$ and $\mathbf{p}_2$. For example, $\mathbf{p}_1$ could be chosen to lie at the OHC-DC junction in some cross-section, and $\mathbf{p}_2$ to lie at the OHC-DC junction in a different cross-section. Note that these points are specified in *optical* coordinates, where $\hat{\mathbf{z}}$ is the optic axis (depth), and $\hat{\mathbf{x}}$ and $\hat{\mathbf{y}}$ are the scanning directions.

While the longitudinal and transverse directions are not constant in space – they change along with the spiral of the cochlea – one can approximate them as being stationary. This amounts to the local approximation of the BM as a plane, which is reasonable over a range of ~ 200 μm[10]. Wehn approximated this way, the line segment connecting anatomical structures of the same type between cross-sections is parallel to the longitudinal axis. That

is, the longitudinal unit vector is given in optical coordinates by

$$\hat{\mathbf{l}} = \frac{\mathbf{p}_2 - \mathbf{p}_1}{||\mathbf{p}_2 - \mathbf{p}_1||}. \tag{6}$$

The component of the measurement axis in the longitudinal direction is simply the $\mathbf{z}$ component of $\hat{\mathbf{l}}$. That is, at each angle $i = 1, 2$, the longitudinal component is

$$l_i = \hat{\mathbf{l}} \cdot \mathbf{z}. \tag{7}$$

Next we recall that the measurement axis $\mathbf{z}_i$ is a *unit* vector, so $t_i^2 + l_i^2 = 1$. This means that

$$t_i = \sqrt{1 - l_i^2}. \tag{8}$$

With this, we have now found the elements of the matrix in Eqn 5. The next goal is to register points to one another between orientations.

For reasons we will motivate shortly, we begin by taking many measurements of the structure of interest along the longitudinal axis. For example, at orientation $i = 1, 2$, if we are interested in the OHC-DC, we find a single point in this region and call it $\mathbf{q}_0$. By the definition of the longitudinal direction, for any real a, $\mathbf{q}_0 + a\hat{\mathbf{l}}$ is also in the OHC-DC region. We choose a number of points N and a spacing δ and take measurements at points

$$\mathbf{q}_n^i = \mathbf{q}_0^i + n\delta\hat{\mathbf{l}}, \; n = 0, 1, \ldots, N. \tag{9}$$

This gives us N measurements of the structure evenly spaced longitudinally. In each measurement line, we inevitably also measure BM at some point $\mathbf{b}_n^i$. As $\mathbf{z} \neq \hat{\mathbf{t}}$, the OHC-DC and BM points measured in each line are not in the same longitudinal cross-section.

8

139 For example, suppose that on the $\mathbf{z}$ axis in a single A-Scan, the BM and OHC-DC are

140 $\Delta = (\mathbf{p}_n^i - \mathbf{b}_n^i) \cdot \mathbf{z}$ apart. Ideally, this value is independent of the cross-section, or n. The

141 cross-sectional distance (i.e. longitudinal distance) between these points is thereby $r^i = \Delta l_i$.

142 Now let's once again consider our first OHC-DC measurement at $\mathbf{q}_0^i$. It is in the same

143 cross-section as a point on the BM at $\mathbf{b}_0^i + r^i \hat{\mathbf{l}}$. We have taken many measurements of BM

144 along the longitudinal axis, so if δ is small, there exists an n such that $r^i \approx n\delta$. That is, $\mathbf{q}_0^i$

145 is approximately in the same cross-section as $\mathbf{b}_n^i$ for this n.

146 We can repeat this process for all measured OHC-DC points to form a list of *aligned*

147 OHC-DC/BM pairs (i.e. OHC-DC and BM in the same cross-section) at each orientation.

148 Using this list, we can reformulate the problem of registering OHC-DC points as one of

149 registering BM points – the OHC-DC points aligned to these BM points would also be

150 registered.

151 To register BM points between orientations, we use the traveling wave to our advantage.

152 To begin, **we assume that the BM moves entirely transversely**. This means that

153 viewed at any angle, the phase response of BM motion will be identical. To register points

154 on the BM between orientations, we compare the phase response at $\mathbf{b}_n^1$ to $\mathbf{b}_m^2$ for $n, m =$

155 $1, 2, \ldots, N$, and find the values for which the phase responses are most similar by minimum

156 L_2 distance.

157 That is, we start by comparing the phase response at $\mathbf{b}_0^1$ to $\mathbf{b}_m^2$ for $m = 0, 1, \ldots, N$, $\phi_0^1(f)$

158 and $\phi_m^2(f)$ respectively where f is frequency. We find

$$m_0 = \operatorname*{argmin}_{m} E_{0,m} = \operatorname*{argmin}_{m} ||\phi_0^1(f) - \phi_m^2(f)||, \tag{10}$$

9

159 and consider $\mathbf{b}_0^1$ and $\mathbf{b}_{m_0}^2$ to be registered. Because BM positions measured are spaced evenly

160 longitudinally by δ in either orientation, this means that $\mathbf{b}_1^1$ and $\mathbf{b}_{m_0+1}^2$ are also registered,

161 and so on.

162 This yields registered BM points across some range of the BM. As we aligned the BM

163 points to OHC points in the previous step, we now have OHC-DC points registered as well.

164 We can then perform our reconstruction.

165 To make this process more concrete, we provide an illustrative example in the Results

166 section below.

167 **C. Error dependence on angular difference**

168 The presentation above is in an ideal environment, wherein the reconstruction can be

169 performed from any two measurements at distinct angles. Mathematically, the error asso-

170 ciated with the angular difference arises from the matrix in Eqn 5. Note that this matrix

171 must be invertible, which require full row rank – i.e. the rows must not be colinear. The

172 rows of this matrix are the measurement axes, $\mathbf{z}_1$ and $\mathbf{z}_2$, which will never be colinear by

173 design. The invertibility of this matrix is thereby guaranteed.

174 However, it is intuitively clear that reconstructions could not be reliably made from two

175 measurements taken, say, $1°$ apart. This lies in the fact that the matrix has a multiplicative

176 impact on the noise in measurements δ_1 and δ_2. As a rule of thumb, if σ_{max} and σ_{min} are

177 the maximum and minimum singular values of a matrix, then matrix multiplication reduces

178   the SNR by a factor of the *condition number*:

$$\kappa = \frac{|\sigma_{max}|}{|\sigma_{min}|}. \tag{11}$$

It can be shown that a matrix and its inverse have the same condition number. The formula for the singular values of a 2×2 matrix (using the element names of the relevant matrix) is known to be

$$\sigma_{max} = \sqrt{\frac{s_1 + s_2}{2}}, \tag{12}$$

$$\sigma_{min} = \sqrt{\frac{s_1 - s_2}{2}}, \tag{13}$$

where

$$s_1 = l_1^2 + t_1^2 + l_2^2 + t_2^2, \tag{14}$$

$$s_2 = \sqrt{(l_1^2 + t_1^2 - l_2^2 - t_2^2) + 4(l_1 l_2 + t_1 t_2)^2}. \tag{15}$$

179

180   We know that the measurement axes are unit vectors, so $l_i^2 + t_i^2 = 1$ for $i = 1, 2$. That

181   gives $s_1 = 2$ and $s_2 = 2(l_1 l_2 + t_1 t_2)$. Defining $\nu = l_1 l_2 + t_1 t_2$, we simplify condition number

182   formula to

$$\kappa = \sqrt{\frac{1 + \nu}{1 - \nu}}, \tag{16}$$

183   a monotonically increasing function of ν.

184   We now note that $\nu = \mathbf{z}_1 \cdot \mathbf{z}_2$, whichmay offer a bit of intuition – the dot product is largest

185   when the two vetors are nearer to parrallel, yielding an increase in condition number. To be

186   more mathematically precise,

$$\nu = ||\mathbf{z}_1|| \, ||\mathbf{z}_2|| \cos \theta = \cos \theta, \tag{17}$$

where θ is the angular distance between the two vectors and we have used the fact that the measurement axes are unit vectors. We now can use double angle trigonometric identities to write the condition number very succinctly as a function of the angular difference between the two measurement axes:

$$\kappa = \sqrt{\frac{1 + \cos\theta}{1 - \cos\theta}} \tag{18}$$

$$= \sqrt{\frac{1}{\tan^2 \frac{\theta}{2}}} \tag{19}$$

$$= \frac{1}{\left| \tan \frac{\theta}{2} \right|}. \tag{20}$$

187

188   The condition number goes to infinity when the angular difference approaches 0, and

189   approaches a minimum at 1 as the angular difference approaches 90°. While 90° would

190   be optimal, the maximum achievable angular difference is restricted by the experimental

191   preparation. For example, in measurements taken through the gerbil round window, 15°

192   is often the largest achievable angular difference. Table I shows condition numbers for a

193   selection of angular deviations achievable in gerbil through the round window membrane.

194   For context, the noise floor of our displacement measurements is approximately 0.1 nm.

195   For a vector of two independent measurements δ_1 and δ_2, our noise floor would thereby

196   be about $\sqrt{0.1^2 + 0.1^2} \approx 0.14$ nm. The noise increase induced by reconstruction using

197   measurements taken 15° (a factor of 7.6, according to Table I) apart would yield a noise

198   floor of $\sim$1 nm.

Angular deviation	Condition number κ
20º	5.67
15º	7.60
10º	11.43
5º	22.90
1º	114.59

TABLE I. A table of condition numbers for the projection matrix at possible measurement angular deviations.

III. RESULTS

We begin with an illustrative example of the method in an *in vivo* gerbil preparation, wherein measurements were taken through the RW. The measurements are then compared to previously measured purely transverse OCC displacements.

A. Illustrative example

We choose to take $N = 11$ measurements at each orientation of the sample, spaced $\delta = 15$ μm apart longitudinally. Viewing the sample at the first orientation, we choose two points at the OHC-DC location,$\mathbf{p}_1^1$ and $\mathbf{p}_2^1$, and take their difference to find the longitudinal axis $\hat{l}^1 = (,,)^T$. We choose $\mathbf{q}_0^1 = \mathbf{p}_1^1$, as we are interested in points at the OHC-DC region. We

208 then take 11 measurements, at $\mathbf{q}_0^1, \mathbf{q}_0^1 + 15\hat{\mathbf{l}}^1, \ldots, \mathbf{q}_0^1 + (11 \times 15)\hat{\mathbf{l}}^1$. Our measurements are made

209 using a 15-frequency Zwuis tone stimulus at several 40, 50, 60, 70 and 80 dB SPL.

210   We repeat this process at the second orientation, where we find $\hat{\mathbf{l}}^2 = (,,)^T$. This gives

211 us all of the measurements we need for the experiment as described in the Methods section,

212 and we can proceed with the mathematical reconstruction.

     The $\hat{\mathbf{z}}^i$-components of the unit longitudinal vectors let us find the measurement matrix

     components from Eqn 5:

$$l_1 =, \ t_1 = \sqrt{1 - l_1^2} = \tag{21}$$

$$l_2 =, \ t_2 = \sqrt{1 - l_2^2} = . \tag{22}$$

213

214   Next, we look at A-Scans at each orientation to find aligned BM and OHC-DC points in

215 the same cross-section. Considering an A-Scan taken at position $\mathbf{q}_0^1$, we see that the OHC-

216 DC junction and BM measurements lie pixels apart. In our system, a pixel is 2.7 μm, so the

217 structures are longitudinally $\Delta =$ apart in the optical axis. This means that they lie $\Delta l_1 =$

218 apart longitudinally. Of all multiples of $\delta = 15$ μm, this value is closest to $= \delta$. That is, this

219 OHC-DC measurement is approximately aligned with the BM measured at $\mathbf{q}_0^1 + \delta\hat{\mathbf{l}} = \mathbf{q}_2^1$.

220 This BM point is $\mathbf{b}_2^1$, i.e. we have aligned OHC-DC $\mathbf{q}_0^1$ with BM $\mathbf{b}_2^1$.

221   This relation holds for the rest of the points measured at this angle, so that the OHC-DC

222 points are generally three runs apart from BM measured in the same A-Scan. This means

223 that OHC-DC $\mathbf{q}_1^1$ is in the same cross-section as BM $\mathbf{b}_3^1$, and so on up to OHC $\mathbf{q}_8^1$ is aligned

224 to $\mathbf{b}_{11}^1$. We can do the same at the second orientation as well to align OHC-DC points and

225 BM points.

226 Now we register BM points between orientations. We start by comparing the phase

227 responses ϕ_0^1 to ϕ_m^2 for $m = 0, 1, \ldots, 10$, and find that the BM from measurement 0 at

228 orientation 1 is best aligned with BM from measurement at orientation 2. This gives us

229 several registered BM pairs, namely . An example of the matched phase responses can be

230 seen in FIGURE, wherein the phase responses of BM points taken at these two orientations

231 are nearly identical.

232 Taking the registered BM points and observing our list of aligned BM and OHC-DC

233 points, we can register several OHC-DC points to one another, namely . We can now

234 perform the mathematical reconstruction at these locations.

235 Reconstructions of longitudinal and transverse motion at the OHC-DC region at 4 posi-

236 tions alongside BM data from the same cross-section are shown in FIGURE. The features

237 of these data are described below.

238 As a note, using the values of l_1, t_1, l_2 and t_2 found above, we see that our measurement

239 axes made and angles with the BM normal at orientations 1 and 2, respectively. The angular

240 difference, , yields a measurement matrix with condition number . This is the factor by which

241 our noise level is increased as a result of our reconstruction.

242 **B. Features of the data and comparison to previous measurements**

243 Observing first the magnitude of the reconstructed data, we see that OHC-DC motion in

244 both the longitudinal and transverse direction are tuned to the same frequency as the BM,

15

245 although less sharply than BM. Both components also show broadband linearity, which is

246 characteristic of past OHC measurements made using tone complex stimuli. Transverse and

247 longitudinal components of motion have similar magnitude at lower SPL, but diverge at 80

248 dB SPL.

249 Observing the phase, the transverse component of OHC-DC motion at SPL lower than

250 80 dB lags BM across frequency by $\sim 0.3 - 0.4$ cycles. At 80 dB SPL and near the best

251 frequency, the OHC-DC transverse component and BM move in phase. The longitudinal

252 component is approximately half a cycle out of phase from transverse displacement across

253 much of the tested frequency range. By the definition of our axes, this means that base-to-

254 apex motion is approximately in phase with Scala Media-to-Scala Tympani motion.

255 To validate our method, we compare to previously measured transverse data. Recent

256 measures from Cho et al and our lab from the hook region are shown in FIGURE. Cho

257 et al's measurements are taken using single-tone stimuli, while ours are taken using Zwuis

258 tone complexes. Comparing to our reconstruction, we can see the following about OHC-

259 DC transverse motion: 1) the motion exhibits broadband nonlinearity when measured using

260 Zwuis tone complexes; 2) it is tuned to the same frequency as BM; 3) at frequencies above 0.5

261 BF, OHC-DC transverse phase lags BM by $\sim$0.3 cycles at lower SPL; 4) at higher SPL near

262 BF, BM and OHC-DC move in phase in measurements taken using Zwuis tone complexes.

263 These characteristic similarities provide evidence that our model is correctly reconstruct-

264 ing these components of motion in the OHC-DC region. In particular, our original puzzle

265 – that OHC-DC re BM phase responses look vastly different when measured from different

266 angles – is resolved by these data.

16

Our reconstruction also indicates that there is a significant component of motion in the longitudinal direction at the OHC-DC junction. As the OHCs are not significantly longitudinally slanted in gerbil (CITE), this is not readily interpreted as a feature of electromotility. Instead, it may indicate the effects of fluid on these structures that is distinct from the more rigid BM, or the impact of other longitudinally tilted processes within the OCC (CITE) on OHC-DC. Study of longitudinal motion in other regions of the OCC could shed more light on the interpretation of measurements such as these.

IV.   EXTENSIONS OF THE METHOD

Here we discuss two theoretical extensions of the method presented here – one in which the accuracy of the method is improved by measuring from more than two longitudinal-transverse angles, and one in which the method is extended to reconstruct all three components of motion. Similar to the presented methods, these techniques require only a single OCT system and do not require any *a priori* knowledge of the measurement angles or precise locations of the structures being measured.

Both proposed extensions require measurements at more than two angles to be taken. This would result in an improvement of the measured data, but would also be significantly more time-consuming and reduce the experiment's yield.

A.   Overdetermined reconstruction

In the method presented above, we take measurements from two angles and solve a deterministic system of two linear equations in two variables. We note the impact of noise

287 in these measurements as it pertains to the condition number of the measurement matrix,

288 which can only be improved via increasing the angular difference between measurement

289 angles.

290 However, one could also improve the accuracy by employing the same experimental

291 method, but measure structures at $M > 2$ angles. We call the measured displacements

292 of a registered structure along these axes $\delta_1, \delta_2, \ldots, \delta_M$ and write the respective measure-

293 ment axes in terms of components $l_1, t_1, l_2, t_2, \ldots, l_M, t_M$. At each registered location, one

294 would now have a system of M equations in 2 variables – an overdetermined system. Math-

295 ematically, we can write the system as follows:

$$y = Ax \tag{23}$$

296

297 As a result of noise, this over-determined system will not have a solution – no value of

298 the true motion **d** can yield all M measured projections. Instead, we must make an *educated*

299 *guess* of the true motion based on our noisy projection measurements.

300 The equation *actually* describing the projection at angle $m = 1, 2, \ldots, M$ is

$$d_l l_m + d_t t_m + \eta_m = \delta_m, \tag{24}$$

301 where η_m is a realization of noise that is different in each measurement, and of course,

302 unknown. Thereby, instead of trying to solve this equation, we try to minimize:

$$\mathcal{E} = \sum_{m=1}^{M} ||\delta_m - (d_l l_m + d_t t_m)||^2. \tag{25}$$

303 The values of d_l and d_t that minimize $\mathcal{E}$ are the least-squares-optimal solution to this overde-

304 termined problem.

305   In general, let $\mathbf{x}$ and $\mathbf{y}$ be vectors and A be a matrix. The least-squares-optimal solution

306   to an overdetermined linear system $\mathbf{y} = A\mathbf{x}$ is $\mathbf{x}_0 = A^\dagger y$, where $A^\dagger$ is the *Moore-Penrose*

307   *pseudoinverse* of A. Most computational software packages include a routine to compute

308   this pseudoinverse (for example, MATLAB's `pinv`.

309   If one wished to employ this version of the method, they would take measurements at M

310   angles along a large longitudinal stretch as described above. They would compute l_m and

311   t_m for each orientation, and register points based on BM phase just as in the two-angle case.

312   At each registered point, they will then reconstruct the true motion via

$$\mathbf{d} = A^\dagger \delta. \tag{26}$$

313   Note that as the pseudoinverse of an invertible matrix is equal to the inverse of said matrix,

314   this equation degenerates to Eqn 5 from the standard method in the $M = 2$ case.

B.   Extension to three dimensions

316   Naturally, after two-dimensional reconstruction, one looks to the third and final spatial

317   dimension – in this case, the radial dimension. To reconstruct three-dimensional motion re-

318   quires motion measurements from three angles, and also requires at least one of our measure-

319   ment axes to have a radial component. This complicates certain steps in our experimental

320   method, but not insurmountably so.

321   First, let's note the 3-D reconstruction formula as a simple generalization of the 2-D

322   formula:

$$\begin{pmatrix} d_l \\ d_r \\ d_t \end{pmatrix} = \begin{pmatrix} l_1 & r_1 & t_1 \\ l_2 & r_2 & t_2 \\ l_3 & r_3 & t_3 \end{pmatrix}^{-1} \begin{pmatrix} \delta_1 \\ \delta_2 \\ \delta_3 \end{pmatrix}, \tag{27}$$

323 where δ_i are the measured displacements at angles $i = 1, 2, 3$, and $\hat{\mathbf{z}}_i = (l_i \, r_i \, t_i)^T$ is the

324 measurement axis at angle i.

325 At each measurement angle, the longitudinal direction can still be computed in the same

326 way, and longitudinally spaced measurements can still be taken along the cochlea just as

327 before. As BM phase response does not vary across radial position within a single cross-

328 section, the registration method can be used just as before.

329 The only difference comes in determining the measurement matrix, which is now 3×3.

330 For this purpose, our previously presented orientation program is well-suited for the task.

331 Given a volume scan at each orientation, this program can be used to approximate the

332 anatomical components of the measurement axis. This would give $\hat{\mathbf{z}}_i$ for $i = 1, 2, 3$, and

333 thereby allow for the complete 3-D reconstruction.

334 Experiments

V. CONCLUSIONS

336 We have presented a method for reconstructing transverse and longitudinal motion in the

337 OCC and provided evidence of its function via comparison of a test data set to previously

338 measured transverse motion measured in the OHC-DC region in gerbil base. This method

339 requires only a single OCT machine, relying on the physiology of the cochlea rather than

340 external hardware.

341 In future, this method could be applied to other regions within the OCC to paint a more

342 complete picture of micromechanical motion – in particular, it may help to understand

343 the impact of longitudinal fluid motion and longitudinally tilted processes in the OCC.

344 Extensions of the method, as presented here, could also be achieve a 3-D profile of intra-
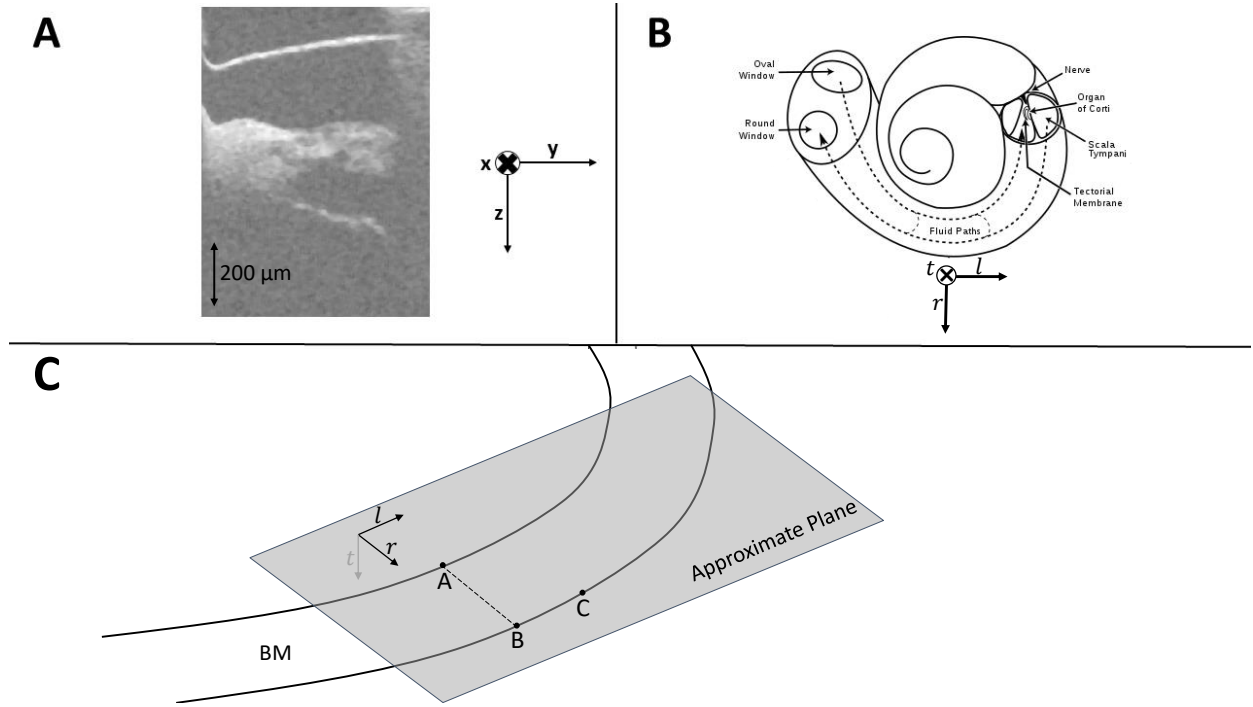
345 OCC motion.

FIG. 1. The coordinate systems used in the development of this program. **A** – the optical co-ordinate system, defined with respect to the orienting B-Scan, shown alongside a representative B-Scan; **B** – the anatomical coordinate frame, which varies so as to always be tangent to the BM at any point, shown at a point along a cartoon of the cochlea; **C** – the local approximation of the anatomical coordinate system, defined with respect to a plane that approximates the BM's plane (shown as a gray surface).

REFERENCES

[1]J. A. Izatt and M. A. Choma, *Theory of Optical Coherence Tomography*, 47–72 (Springer Berlin Heidelberg, Berlin, Heidelberg), https://doi.org/10.1007/978-3-540-77550-8_2, doi: 10.1007/978-3-540-77550-8_2.

[2]M. A. Choma, A. K. Ellerbee, C. Yang, T. L. Creazzo, and J. A. Izatt, "Spectral-domain phase microscopy," Opt. Lett. **30**(10), 1162–1164 (2005) http://ol.osa.org/abstract.cfm?URI=ol-30-10-1162 doi: 10.1364/OL.30.001162.

[3]S. S. Gao, R. Wang, P. D. Raphael, Y. Moayedi, A. K. Groves, J. Zuo, B. E. Applegate, and J. S. Oghalai, "Vibration of the organ of corti within the cochlear apex in mice," Journal of neurophysiology **112** (2014) doi: 10.1152/jn.00306.2014.

[4]W. Dong, A. Xia, P. D. Raphael, S. Puria, B. E. Applegate, and J. S. Oghalai, "Organ of corti vibration within the intact gerbil cochlea measured by volumetric optical coherence tomography and vibrometry," Journal of Neurophysiology **120** (2018) doi: 10.1152/jn.00702.2017.

[5]E. Fallah, C. E. Strimbu, and E. S. Olson, "Nonlinearity and amplification in cochlear responses to single and multi-tone stimuli," Hearing Research **377**, 271–281 (2019) doi: 10.1016/j.heares.2019.04.001.

[6]C. E. Strimbu, Y. Wang, and E. S. Olson, "Manipulation of the endocochlear potential reveals two distinct types of cochlear nonlinearity," Biophysical Journal **119**(10), 2087–2101 (2020) https://www.sciencedirect.com/science/article/pii/S0006349520308055 doi: https://doi.org/10.1016/j.bpj.2020.10.005.

[7]F. Chen, D. Zha, A. Fridberger, J. Zheng, N. Choudhury, S. L. Jacques, R. K. Wang, X. Shi, and A. L. Nuttall, "A differentially amplified motion in the ear for near-threshold sound detection," Nature Neuroscience **14**(6), 770–774 (2011) doi: 10.1038/nn.2827.

[8]H. Y. Lee, P. D. Raphael, A. Xia, J. Kim, N. Grillet, B. E. Applegate, A. K. E. Bowden, and J. S. Oghalai, "Two-dimensional cochlear micromechanics measured in vivo demonstrate radial tuning within the mouse organ of corti," Journal of Neuroscience **36**(31), 8160–8173 (2016) doi: 10.1523/jneurosci.1157-16.2016.

[9]N. P. Cooper, A. Vavakou, and M. Van Der Heijden, "Vibration hotspots reveal longitudinal funneling of sound-evoked motion in the mammalian cochlea," Nature Communications **9**(1), 3054 (2018) doi: 10.1038/s41467-018-05483-z.

[10]B. L. Frost, C. E. Strimbu, and E. S. Olson, "Using volumetric optical coherence tomography to achieve spatially resolved organ of corti vibration measurements," Journal of the Acoustical Society of America **151**, 1115–1125 (2022).

[11]N. P. Cooper, A. Vavakou, and M. van der Heijden, "Vibration hotspots reveal longitudinal funneling of sound-evoked motion in the mammalian cochlea," Nature Communications **9**, 3054 (2018).

[12]N. H. Cho and S. Puria, "Motion of the cochlear reticular lamina varies radially across outer-hair-cell rows," bioRxiv (2022) https://www.biorxiv.org/content/early/2022/03/04/2022.03.01.482580 doi: 10.1101/2022.03.01.482580.